Three-dimensional multi-fluid simulations of Pluto's magnetosphere: A comparison to 3D hybrid simulations

E. M. Harnett and R. M. Winglee

Department of Earth and Space Sciences, University of Washington, Seattle, Washington, USA

P. A. Delamere

Laboratory for Atmospheric and Space Physics, University of Colorado, Boulder, Colorado, USA

Received 14 April 2005; revised 22 August 2005; accepted 1 September 2005; published 11 October 2005.

[1] Results from 3D multi-fluid simulations of the solar wind interaction with Pluto are compared to 3D hybrid simulations of the same interaction. The results from the multi-fluid simulations are similar to the hybrid results in both the overall size of the magnetosphere as well as predicting pick-up of ionospheric ions by the solar wind. The results from the multi-fluid simulations also show how an increase in the mass of the pick-up ion leads to a larger pick-up region and an asymmetric bow shock. When the solar wind speed is doubled, but its dynamic pressure is held constant, the size of the magnetosphere more than doubles and the asymmetry of the bow shock and pick up region are enhanced. This effect is not present in MHD simulations since ion cyclotron effects are neglected. The results illustrate the ability of the multi-fluid technique to capture ion cyclotron effects, like the hybrid technique.
Citation: Harnett, E. M., R. M. Winglee, and P. A. Delamere (2005), Three-dimensional multi-fluid simulations of Pluto's magnetosphere: A comparison to 3D hybrid simulations, *Geophys. Res. Lett.*, *32*, L19104, doi:10.1029/2005GL023178.

1. Introduction

[2] The interaction of unmagnetized planets with the solar wind will be controlled by the solar wind interaction with the ionosphere and exosphere. Thus the solar wind interaction will be effected by ion pick-up. Exospheric ions can be accelerated (and picked up) in the direction of the convection electric field. When these ions gyrate outside of the bow shock, charge neutrality dictates that the solar wind move inward, leading to an asymmetric bow shock. Hall currents can lead to additional asymmetries [cf. *Brecht*, 1997].

[3] Both ionospheric pickup and an asymmetric bow shock have been observed at Venus [*Luhmann et al.*, 1985; *Phillips et al.*, 1987]. As the solar wind hydrogen ion inertial length is roughly two times Pluto's radius, it is possible that a bow shock does not form around Pluto as the scale size of the interaction region is too small for compressional waves to form. 2.5D hybrid and bi-ion fluid simulations of the interaction region around comet-like objects [*Hopcroft and Chapman*, 2001; *Sauer et al.*, 1997; *Lipatov et al.*, 1997] showed asymmetries in the ion pickup region, but that the extent of the asymmetry and the formation of a bow shock depended on the gas production rate of the object. 2D bi-ion fluid simulations [*Bogdanov et al.*, 1996], and 3D hybrid simulations of comet-like objects at 1 AU [*Lipatov et al.*, 2002], showed that a bow shock formed for production rates an order of magnitude smaller. Using a 3D hybrid model to simulate the solar wind interaction with Pluto, *Delamere and Bagenal* [2004] found that even smaller production rates lead to the formation of a bow shock, as the solar wind is more tenuous and the IMF weaker at Pluto than at 1 AU. They also found that the bow shock would be highly asymmetric due to ion pick-up processes.

[4] This paper presents results from 3D multi-fluid simulations for the solar wind interactions with Pluto. Pluto's magnetosphere was chosen due to its highly kinetic nature. This will test the robustness of the 3D multi-fluid technique. A comparative study is important as hybrid simulations provide a treatment that includes full ion dynamics but with limited spatial resolution and system size. The fluid simulations exclude effects from non-Maxwellian ion populations but allow for higher grid resolution and larger system sizes. The multi-fluid simulations also have a higher dynamic range in density so the full extent of the ion pick up region can be more easily identified. The results detail the ability of the multi-fluid treatment to capture critical ion cyclotron effects seen in hybrid simulations, the 2D two ion fluid simulations by *Harold and Hassam* [1994] and the 2D bi-ion fluid simulations by *Sauer et al.* [1997].

[5] The 3D multi-fluid treatment is also used to demonstrate how changes in the solar wind/ionospheric conditions yield variations in the shape of Pluto's magnetosphere. Asymmetries in the shape will be caused by both mass loading of the solar wind and the Hall effect. This paper discusses the changes caused by variations in mass loading due to ion cyclotron effects.

2. Model

[6] Any number of species can be assumed in the multi-fluid model, with the limits being computation speed. Following the assumptions of *Delamere and Bagenal* [2004], two ion populations were used, a hydrogen solar wind and an ionosphere of N_2^+. A detailed discussion of the multi-fluid technique as applied to the Earth's magnetosphere can be found in *Winglee* [2004]. The multi-fluid equations are:

$$\frac{\partial \rho_i^m}{\partial t} + \nabla \cdot \left(\rho_i^m \mathbf{v}_i\right) = 0 \quad (1)$$

0094-8276/05/2005GL023178

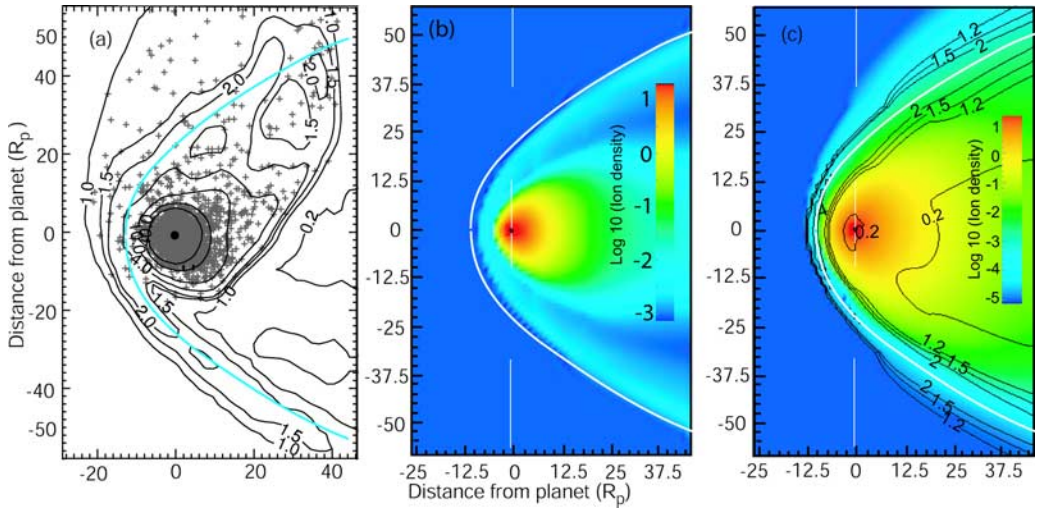

Figure 1. Figure (a) shows the relative solar wind ion density (contour lines) and position of ionospheric ions (pluses) for 3D hybrid simulations by *Delamere and Bagenal* [2004]. Figure (c) shows the relative solar wind density (black contours) and the log of the ionospheric density (color) for the multi-fluid simulations. Figure (b) is from ideal MHD simulations, and only the log of ion density is shown. For (b) and (c), the ionospheric density is in $\log_{10}(\mathrm{cm}^{-3})$. In all three cases the mass of the ionospheric ion is assumed to be $10\mathrm{m_p}$.

$$\rho_i^{\mathrm{m}} \frac{\mathrm{d}\mathbf{v}_\mathrm{i}}{\mathrm{dt}} = q_i n_i (\mathbf{E} + \mathbf{v}_i \times \mathbf{B}) - \nabla P_i + \rho_i^m \mathbf{g}(\mathbf{r}) \tag{2}$$

$$\frac{\partial \mathrm{P_i}}{\partial t} = -\gamma \nabla \cdot (\mathrm{P_i}\mathbf{v_i}) + (\gamma - 1)\mathbf{v_i} \cdot \nabla \mathrm{P_i} \tag{3}$$

$$\frac{\partial \mathrm{P_e}}{\partial t} = -\gamma \nabla \cdot (\mathrm{P_e}\mathbf{v_{de}}) + (\gamma - 1)\mathbf{v_{de}} \cdot \nabla \mathrm{P_e} \tag{4}$$

$$\frac{\partial \mathbf{B}}{\partial t} + \nabla \times \mathbf{E} = 0 \tag{5}$$

$$\mathbf{J} = \nabla \times \mathbf{B} \tag{6}$$

$$n_e = \sum_i n_i \tag{7}$$

$$\mathbf{v}_{de} = \sum_i \frac{n_i}{n_e}\mathbf{v}_i - \frac{\mathbf{J}}{en_e} \tag{8}$$

$$\mathbf{E} = -\sum_i \frac{n_i}{n_e}\mathbf{v}_i \times \mathbf{B} + \eta \mathbf{J} + \frac{1}{en_e}(\mathbf{J} \times \mathbf{B} - \nabla P_e) \tag{9}$$

where ρ_i^{m} is the mass density, n_i the number density, q_i charge, $\mathbf{v}_i$ the bulk velocity, and $\mathrm{P_i}$ the pressure, for each individual ion species i. $\mathrm{P_e}$ is the electron pressure, which is initialized at one half the hydrogen pressure. $\mathrm{n_e}$ is the electron number density, e the electron charge, and $\mathbf{v}_{de}$ the electron drift speed. $\mathbf{g}(\mathbf{r})$ is the gravitational vector, $\mathbf{J}$ the current density, $\mathbf{B}$ the magnetic field, and $\mathbf{E}$ the electric field. γ is the ratio of specific heats and equal to $\frac{5}{3}$. The resistivity (η) is non-zero and equal to 10^3 ohm m^{-1}only inside the inner boundary, and the $\mathbf{J} \times \mathbf{B}$ and ∇P_e terms are only evaluated outside the inner boundary.

[7] Equations (1)–(9) are equivalent to those used in hybrid simulations except the equations for the ions are in the fluid limit. This formalism is similar to that used by *Harold and Hassam* [1994], albeit in three dimensions instead of two. It is also similar to the 2D bi-ion fluid formalism presented in *Bogdanov et al.* [1996] and *Sauer et al.* [1997], except that the bi-ion approach neglected Hall effects.

[8] Note that equation (9) includes the Hall and pressure gradient corrections to the ideal Ohm's law. The ratio of these two terms relative to the convection electric field is defined as R_s. R_s is also of the same order as the ratio of the ion skin depth to the inherent scale length of a given current layer thickness [*Winglee*, 2004]. This inherent scale length can not be smaller than the grid spacing. For Pluto, R_s is of the order of unity and hence the need to include non-ideal MHD effects.

[9] The influence of ion cyclotron effects on the momentum equation can be seen by substituting equation (9) into equation (2) which yields

$$\rho_i^{\mathrm{m}} \frac{\mathrm{d}\mathbf{v}_\mathrm{i}}{\mathrm{dt}} = q_i n_i \left[(\mathbf{v}_i \times \mathbf{B}) - \sum_i \frac{n_i}{n_e}(\mathbf{v}_i \times \mathbf{B}) \right] + \mathbf{J} \times \mathbf{B} - \nabla(P_i + P_e) + \rho_i^m \mathbf{g}(\mathbf{r}) \tag{10}$$

The sum of the first two terms on the right hand side of equation (10) is equal to zero in MHD, as it is assumed that all ions have the same bulk motion. In the presence of finite ion cyclotron effects, this term is non-zero and yields the asymmetric behavior described in the following. This correction, like those in the Ohm's law, is of the order of R_s.

[10] The multi-fluid simulations solve the above equations in 3D on a nested grid system, with 3 grids each centered about the equator and noon meridian. The coordinates are such that $\vec{x}$ is parallel to the solar wind velocity, and $\vec{z}$ is perpendicular to the ecliptic plane. The resolution of the multi-fluid simulations is 358 km near Pluto, increasing to 1433 km away from Pluto. This compares with the fixed resolution of 2200 km given by *Delamere and Bagenal* [2004]. The ratio of the ion skin depth relative to the finest

Table 1. Parameters for Four Different Case Studies[a]

	Ionospheric Ion Mass, m_p	Solar Wind Density, cm^{-3}	Solar Wind Speed, km s^{-1}
Case A	10	0.01	450
Case B	28	0.01	450
Case C	10	0.0025	900
Case D	28	0.0025	900

[a]In all the cases, the dynamic pressure of the solar wind is held constant at 3.4×10^{-12} Pa, and B_z is equal to 0.2 nT.

grid spacing is of the order of unity. The inner boundary is set at an altitude of 1000 km (with R_P equal to 1150 km). The N_2^+ number density at the inner boundary is set to 200 cm^{-3}, with a temperature of 1000 K, and a scale height of 800 km [*Ip et al.*, 2000]. The solar wind density is 0.01 ions cm^{-3}, with a speed of 450 km/s, and the IMF is 0.2 nT in the $+B_z$ direction. The multi-fluid simulations were run for 6–8 transit times.

3. Comparisons Between Multi-Fluid and Hybrid Simulations

[11] Figure 1 shows a comparison between hybrid simulations, ideal MHD simulations and multi-fluid simulations. The solar wind and ionospheric densities are shown in the plane perpendicular to the IMF direction (i.e. the xy plane). Figure 1a shows the results from *Delamere and Bagenal* [2004]. It is seen that the pickup of heavy ions due to ion cyclotron effects is preferentially to the top of Figure 1a and this leads to an asymmetric bow shock. This change in the bow shock is due to the fact that the electrons remain magnetized. As such, when the heavy ions with their much larger ion gyro-radii are picked up, the solar wind ions must be pulled inward in order to maintain quasi-neutrality. On the opposite side the bow shock moves out to maintain momentum conservation.

[12] Figure 1b shows the results of ideal MHD simulations. The model is described in *Harnett and Winglee* [2003] and run in ideal MHD mode. This is equivalent to setting the sum of the first two terms in equation (10) and the last two terms in equation (9) equal to zero, for a single species. As the simulations are a single fluid simulation, only the density of the one ion species is shown. The mass density at the inner boundary was held at the same value as in the multi-fluid simulations, and is accounted for by plotting the effective number density. In the ideal MHD case there is no ion pick up region outside the bow shock.

[13] Figure 1c shows the results for when the R_s is set to 0.7 and all the terms in equation (10) and equation (9) are evaluated. In this case, a pick up region develops beyond the bow shock, similar to the hybrid simulations. The subsolar point of the bow shock is at $10R_P$. In comparison, the bow shock subsolar point is at $7.5R_P$ in the ideal MHD simulations and $12R_P$, as measured to the outer edge of the solar wind contour equal to 4.0, in the hybrid simulations. The difference of $2R_P$ corresponds to 1 grid point in the hybrid simulation and ~2 of the coarsest grid points in the multi-fluid simulation. At $42R_P$ downstream, the outer edge of the bow shock is $57R_P$ from the axis running through noon and midnight, on the dawn side (upper portion of Figure 1c) and $58R_P$ on the dusk side (lower portion) - the bow shock is essentially symmetric.

[14] The white curve in Figure 1c indicates the approximate shape of the bow shock. The curve is replicated in Figure 1b at the same position as in Figure 1c. It is also shown in Figure 1a in blue but with the position relative to the planet moved one grid point out to account for the difference in the sub-solar point in the hybrid simulations. The main difference between the multi-fluid and hybrid simulations is that in the hybrid simulations some of the pick up ions are further out in the solar wind. As a result, the bow shock in the pick-up region is closer to the planet and on the opposite side it is further from the planet. This difference is most likely due to the presence of a high-energy tail in the ion distribution in the hybrid simulations that is not incorporated in the multi-fluid simulations. In the hybrid simulations, the distributions in the bow shock are generally half or partial ring beam distributions. Similar distributions were seen by *Kecskemety and Cravens* [1993] using a particle tracking method. A similar qualitative agreement between 2D hybrid and 2D bi-ion fluid simulations of the solar wind interaction with Pluto was also found by *Sauer et al.* [1997]. The effects of non-

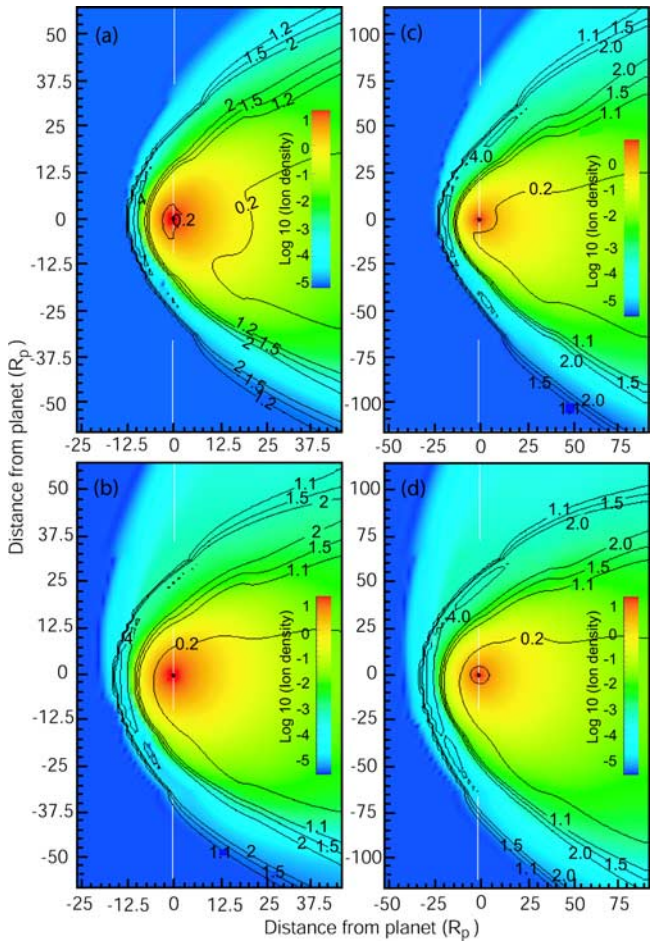

Figure 2. The solar wind density (black contours) and the log of the ionospheric density (color) in the xy plane for the cases in Table 1.

Maxwellian distributions will be investigated in future simulations.

4. Variance With Solar Wind Conditions

[15] With the above calibrations, we can now evaluate how the size of the pick up region and the asymmetry in the bow shock are influenced by changes in the solar wind conditions and the composition of the ions from Pluto. Table 1 shows the parameters for four different case studies, and the corresponding changes in the magnetosphere are shown in Figure 2. Figures 2a–2d are of the same form as in Figure 1, and Figure 2a is identical to Figure 1c.

[16] Figures 2a and 2b show the effect of the mass of the planetary ion species on the pick-up process. Due to computational limitations, the mass of the ionospheric N_2^+ ion was set to $10m_p$ in the hybrid simulations. There is not a similar difficulty in the multi-fluid technique. Increasing the mass of the ionospheric ion from $10m_p$ to $28m_p$, while keeping the solar wind density and velocity and the ionospheric number density fixed, leads to an increase in the size of the magnetosphere. The sub-solar point of the bow shock is now at $13R_P$ (Figure 2b). A definitively asymmetric bow shock forms. The size of the pick up region is also much larger for the heavy ion case (Case B) than the light ion case (Case A) because the cyclotron radius is bigger. Therefore the solar wind will be pulled further in, resulting in a bow shock forming closer to the surface on the pick-up side. At $42R_P$ downstream, the bow shock on the ion pick up side now forms at $55R_P$ from the noon-midnight axis, while it forms at $63R_P$ on the opposite side - closer to the planet on the pick-up side and further from the planet on the opposite side, when compared to Case A. Inside the pick-up region, and outside the bow shock, the speed of the solar wind is reduced to 350–400 km s^{-1}, slower than the incident solar wind but still supersonic. In the same region, the heavy ion speed is on the same order as the solar wind speed. As the ions travel downstream, outside of the bow shock, they are accelerated up to the undisturbed solar wind speed.

[17] Pick-up is also a function of the convection electric field. To test this aspect, the solar wind velocity was doubled in Cases C and D. To keep the dynamic pressure the same as in Cases A and B, the solar wind density was reduced by a factor of 4. The IMF strength and the heavy ion masses remain the same. For a purely MHD interaction, the constant dynamic pressure would indicate that the bow shock in Case C (Figure 2c) should be in the same position as in Case A, while the slight increase in the magnetosonic mach number would suggest that the bow shock will form closer to the planet. Instead, the magnetosphere is nearly double the size in Case A, with the bow shock subsolar point at $19R_P$. And note that while the pick-up regions and bow shocks in Figures 2a and 2c look similar, the area shown in Figure 2c is twice that in Figure 2a. This again is due to pick-up. Doubling the solar wind velocity, increases the electric field and the speed of the pick-up ions, which in turn increases their cyclotron radius and the size of the pick-up region. The size of the pick-up region more than doubles, meaning that the process is non-linear. This also means the bow shock is slightly more asymmetric. In Case C, the edge of the bow shock is measured $83R_P$ downstream to account for the factor of 2 increase in the size of the magnetosphere. On the pick-up side, the edge of the bow shock is 112 R_P from the noon-midnight axis, less than twice the distance in Case A. On the opposite side, the bow shock is $122R_P$ from the noon-midnight axis, more than twice the distance in Case A.

[18] This behavior is also true for the heavy ion cases (Case D relative to Case B). When the solar wind velocity is doubled for the heavy ion case, the position of the sub-solar point of the bow shock moves from $13R_P$ to $26R_P$ (Figure 2d), and the size of the pick-up region more than doubles. Accordingly, the bow shock is more asymmetric than in Case B. The edge of the bow shock at $83R_P$ downstream is $100R_P$ and $138R_P$ from the noon-midnight axis for the upper and lower portions, respectively.

5. Summary

[19] In this paper we have shown that the 3D multi-fluid treatment is able to capture key ion cyclotron effects for the interaction of the solar wind at Pluto. Hybrid simulations have shown the development of an asymmetric bow shock in the presence of the pick up of heavy ions from Pluto, which can extend well beyond Pluto's magnetosphere. Both the pick-up region and the asymmetry in the bow shock is captured in the multi-fluid treatment, although the pick-up region is smaller in the latter. This difference is most likely due to the fact that the multi-fluid treatment excludes the presence of higher energy tails in the particle distributions whereas such populations can be generated in hybrid codes.

[20] But the multi-fluid treatment does allow for a more extensive examination of the controlling influences such as the composition of the pick up ions from Pluto. Increasing the mass of the heavy ions leads to an increase in the size of Pluto's magnetosphere, while increasing the asymmetry in the bow shock and pick up region. And the influence of the heavy ion mass is as strong as the solar wind conditions.

[21] The results show that the multi-fluid treatment can be an important complement to hybrid simulations. Hybrid simulations incorporate full ion dynamics but have limited grid resolution and system size, and are computationally expensive to run. The multi-fluid simulations incorporate many of the same ion cyclotron effects, albeit with some missing dynamics due to the presence of high energy tails. Multi-fluid simulations are computationally cheaper to run, thereby allowing for a more detailed study of controlling influences with higher grid resolution and larger system sizes.

References

Bogdanov, A. S., et al. (1996), Plasma structures at weakly outgassing comets—Results from bi-ion fluid analysis, *Planet. Space Sci.*, *44*, 519–528.

Brecht, S. (1997), Hybrid simulations of the magnetic topology of Mars, *J. Geophys. Res.*, *102*, 4743–4750.

Delamere, P. A., and F. Bagenal (2004), Pluto's kinetic interaction with the solar wind, *Geophys. Res. Lett.*, *31*, L04807, doi:10.1029/2003GL018122.

Harnett, E. M., and R. M. Winglee (2003), The influence of the mini-magnetopause on the magnetic pileup boundary at Mars, *Geophys. Res. Lett.*, *30*(20), 2074, doi:10.1029/2003GL017852.

Harold, J. B., and A. B. Hassam (1994), Two ion fluid numerical investigations of solar wind gas releases, *J. Geophys. Res.*, *99*(A10), 19,325–19,340.

Hopcroft, M. W., and S. C. Chapman (2001), 2D hybrid simulations of the solar wind interaction with a small scale comet in high Mach number flows, *Geophys. Res. Lett.*, *28*, 1115–1118.

Ip, W.-H., et al. (2000), Pluto's ionospheric models and solar wind interaction, *Adv. Space Res.*, *26*, 1559–1563.

Kecskemety, K., and T. E. Cravens (1993), Pick-up ions at Pluto, *Geophys. Res. Lett.*, *20*, 543–546.

Lipatov, A. S., et al. (1997), 2.5D hybrid code simulation of the solar wind interaction with weak comets and related objects, *Adv. Space Res.*, *20*, 279–282.

Lipatov, A. S., et al. (2002), 3D hybrid simulations of the solar wind interaction with a weak comet, *Planet. Space Sci.*, *50*, 403–411.

Luhmann, J. G., et al. (1985), Evidence for mass-loading of the Venus magnetosheath, *Adv. Space Res.*, *5*(4), 307–311.

Phillips, J. L., et al. (1987), Finite Larmor radius effects on ion pickup at Venus, *J. Geophys. Res.*, *92*, 9920–9930.

Sauer, K., et al. (1997), Solar wind-Pluto interaction revised, *Adv. Space Res.*, *20*, 295–299.

Winglee, R. M. (2004), Ion cyclotron and heavy ion effects on reconnection in a global magnetotail, *J. Geophys. Res.*, *109*, A09206, doi:10.1029/2004JA010385.

E. M. Harnett and R. M. Winglee, Department of Earth and Space Science, Box 351310, University of Washington, Seattle, WA 98195-1310, USA. (eharnett@ess.washington.edu; winglee@ess.washington.edu)

P. A. Delamere, Laboratory for Atmospheric and Space Physics, CB 392 Duane Physics, University of Colorado, Boulder, CO 80309-0391, USA. (delamere@lasp.colorado.edu)